

Journal of Petroleum & Chemical Engineering

https://urfpublishers.com/journal/petrochemical-engineering

Vol: 3 & Iss: 3

Analysis and Control of the Lorenz 84 Atmospheric Circulation Model

Lakshmi N. Sridhar*

Chemical Engineering Department, University of Puerto Rico, Mayaguez, PR 00681, USA

Citation: Sridhar LN. Analysis and Control of the Lorenz 84 Atmospheric Circulation Model. *J Petro Chem Eng* 2025;3(3):167-173.

Received: 06 September, 2025; Accepted: 08 September, 2025; Published: 10 September, 2025

*Corresponding author: Lakshmi N. Sridhar, Chemical Engineering Department, University of Puerto Rico, Mayaguez, PR 00681, USA, Email: lakshmin.sridhar@upr.edu

Copyright: © 2025 Sridhar LN., This is an open-access article published in J Petro Chem Eng (JPCE) and distributed under the terms of the Creative Commons Attribution License, which permits unrestricted use, distribution, and reproduction in any medium, provided the original author and source are credited.

ABSTRACT

Atmospheric models exhibit complex dynamical behaviors and it is important to understand the dynamics of atmospheric circulation so that strategies to control the circulation can be developed in the future. In this work, bifurcation analysis and multiobjective nonlinear model predictive control is performed on the Lorenz-84 atmospheric circulation model. Bifurcation analysis is a powerful mathematical tool used to deal with the nonlinear dynamics of any process. Several factors must be considered and multiple objectives must be met simultaneously. The MATLAB program MATCONT was used to perform the bifurcation analysis. The MNLMPC calculations were performed using the optimization language PYOMO in conjunction with the state-of-the-art global optimization solvers IPOPT and BARON. The bifurcation analysis revealed the existence of a Hopf bifurcation point and a limit point. The MNLMC converged to the utopia solution. The Hopf bifurcation point, which causes an unwanted limit cycle, is eliminated using an activation factor involving the tanh function. The limit point (which cause multiple steady-state solutions from a singular point) are very beneficial because it enables the Multiobjective nonlinear model predictive control calculations to converge to the Utopia point (the best possible solution) in the model.

Keywords: Bifurcation; Optimization; Control; Atmospheric circulation

Background

Atmospheric circulation dynamics represent one of the most complex and fascinating systems on Earth, emerging from the intricate interplay of physical laws, energy exchanges and feedback loops that span across spatial and temporal scales. At its core, atmospheric circulation is the global movement of air that redistributes energy from regions of surplus, primarily near the equator, to regions of deficit, primarily toward the poles. This redistribution moderates' temperatures, drives weather systems and sustains climates that make life on Earth possible. However, the underlying mechanisms are far from simple. They are governed by nonlinear interactions between radiation, pressure gradients, the rotation of the Earth, friction, latent heat

release and the thermodynamic properties of air and water vapor. This complexity gives rise to emergent patterns such as jet streams, trade winds, monsoons and cyclones, whose behavior is predictable in some aspects yet chaotic in others. Understanding atmospheric circulation therefore requires not only physics but also mathematics, fluid dynamics and even chaos theory to capture its multifaceted nature.

The driving force of atmospheric circulation begins with solar radiation, which is unevenly distributed across the planet's surface. The equatorial regions receive more direct solar energy, creating a surplus of heat, while higher latitudes receive less energy due to the curvature of the Earth and the angle of incidence

of sunlight. This imbalance sets the stage for atmospheric motion as nature seeks equilibrium through the transport of energy. Heated air near the equator rises, creating regions of low pressure, while cooler, denser air from higher latitudes moves in to replace it. In theory, this would create a simple one-cell system per hemisphere, with air rising at the equator and sinking at the poles. However, the Earth's rotation and the conservation of angular momentum complicate this simple picture.

The Coriolis effect, a consequence of the Earth's rotation, deflects moving air masses to the right in the Northern Hemisphere and to the left in the Southern Hemisphere. This effect fragments the idealized single-cell circulation into three distinct cells per hemisphere: the Hadley cell, the Ferrel cell and the Polar cell. Each cell represents a general pattern of rising, poleward flow aloft, sinking and equatorward return flow near the surface, but the reality is far more irregular. The Hadley cell dominates tropical latitudes, where warm air rises near the equator, diverges aloft and descends near 30 degrees latitude, creating subtropical high-pressure zones associated with deserts. The Ferrel cell, spanning midlatitudes, is indirectly driven and acts more like a gear between the Hadley and Polar cells, with surface westerlies resulting from the balance of forces rather than direct thermal forcing. The Polar cell completes the system, with cold air sinking at the poles and moving equatorward. Yet these idealized structures are constantly perturbed by planetary waves, ocean-atmosphere interactions and transient weather systems.

Embedded within these circulation cells are jet streams, narrow bands of fast-moving air in the upper atmosphere. Jet streams arise from strong temperature gradients, particularly near the boundaries of circulation cells and are intensified by the Coriolis effect. The polar jet stream, for example, separates cold polar air from warmer midlatitude air and plays a central role in steering storm systems. These jets do not flow smoothly around the globe but meander due to the presence of Rossby waves, large-scale undulations in the westerlies caused by the conservation of potential vorticity. These meanders can amplify into blocking patterns that disrupt typical weather, leading to prolonged heatwaves, cold spells or heavy rainfall. The dynamics of jet streams and Rossby waves highlight the nonlinear, quasi-chaotic nature of atmospheric circulation, where small perturbations can cascade into large-scale anomalies with significant societal impacts.

Moisture further complicates circulation dynamics. Water vapor is a potent greenhouse gas and its phase changes involve latent heat exchanges that strongly influence atmospheric motion. In the tropics, convection and the release of latent heat drive towering cumulonimbus clouds and contribute to the maintenance of the Hadley circulation. Monsoon systems exemplify this coupling of heat and moisture, where seasonal shifts in land-sea temperature contrast drive massive, periodic reorganizations of atmospheric circulation and precipitation. The South Asian monsoon, for instance, arises when the landmass heats more rapidly than the surrounding ocean, creating a pressure gradient that pulls moist oceanic air inland, where it rises, cools and releases torrential rainfall. These systems are sensitive to subtle changes in surface conditions, illustrating the delicacy of feedbacks in circulation dynamics.

Atmospheric circulation is also deeply intertwined with ocean circulation, forming the coupled climate system. Ocean

currents redistribute heat, while sea surface temperatures influence atmospheric pressure patterns and wind fields. Phenomena such as El Niño—Southern Oscillation (ENSO) reveal the tight coupling between ocean and atmosphere. During El Niño events, weakened trade winds allow warm waters to spread across the equatorial Pacific, altering convection and triggering teleconnections that disrupt weather patterns worldwide. Conversely, La Niña events enhance trade winds and intensify the normal circulation. These oscillations showcase how atmospheric circulation is not confined to local scales but resonates across the globe, producing variability that challenges prediction.

The complexity of atmospheric circulation dynamics is further underscored by the influence of turbulence and chaos. On smaller scales, turbulent eddies mix heat, moisture and momentum, shaping boundary layer processes that affect everything from cloud formation to pollutant dispersion. On larger scales, the nonlinear equations governing atmospheric motion, particularly the Navier–Stokes equations adapted for a rotating, stratified fluid, admit chaotic solutions. Edward Lorenz's pioneering work demonstrated how tiny differences in initial conditions could lead to vastly different outcomes, a phenomenon popularly known as the butterfly effect. This sensitivity limits deterministic prediction of weather beyond a few weeks, underscoring the inherent unpredictability within a system governed by deterministic laws.

Despite this unpredictability at short timescales, atmospheric circulation exhibits robust patterns on longer timescales, such as the quasi-biennial oscillation in equatorial stratospheric winds or the North Atlantic Oscillation in midlatitude pressure patterns. These modes of variability reflect the system's tendency to self-organize around certain preferred states, even amid chaotic fluctuations. Climate change introduces an additional layer of complexity, as anthropogenic greenhouse gas emissions alter radiative balances, surface temperatures and circulation patterns. The expansion of the Hadley cell, shifts in jet stream behavior and changes in monsoon dynamics are all observed or projected responses to a warming world, with profound implications for ecosystems and human societies.

To grapple with this complexity, scientists employ a range of tools, from observational networks using satellites, balloons and ground stations, to theoretical models and numerical simulations. General circulation models (GCMs) attempt to simulate the atmosphere by discretizing the governing equations over a three-dimensional grid, incorporating processes such as radiation, convection and cloud formation. Yet no model can capture all scales of motion, leading to uncertainties, especially in representing sub-grid processes like turbulence and cloud microphysics. Advances in computational power and data assimilation continue to refine predictions, but the fundamental nonlinear, coupled nature of atmospheric circulation ensures that uncertainty will always remain a part of the picture.

Ultimately, atmospheric circulation dynamics illustrate the beauty and difficulty of understanding complex systems. What begins as the simple physical principle of uneven solar heating unfolds into a network of interacting processes spanning scales from turbulent eddies to planetary waves. The system is simultaneously ordered and chaotic, predictable and unpredictable, resilient and sensitive. It sustains climates, shapes ecosystems and governs the weather patterns that societies

depend on, yet it defies complete mastery. Appreciating this complexity requires not only scientific rigor but also humility in recognizing the limits of prediction. The atmosphere is a dynamic, living system, constantly evolving under the laws of physics yet producing emergent behaviors that continue to challenge and inspire human inquiry.

Nicolis¹ discussed the solar variability and stochastic effects on climate. Benzi, et al.² researched the stochastic resonance in climate change. Nicolis³ described the stochastic aspects of climatic transitions in response to a periodic forcing. Lorenz⁴ showed that irregularity was a fundamental property of the atmosphere. Shilnikov, et al.5 provided the bifurcation and predictability analysis of a low-order atmospheric circulation model. Roebber⁶, discussed the climate variability in a low-order coupled atmosphere-ocean model. Pelino, et al.7 demonstrated the dissipation in Lie-Poisson systems and the Lorenz-84 model. Broer, et al.⁸ showed the existence of bifurcations and strange attractors in the Lorenz-84 climate model with seasonal forcing. Van Veen⁹, discussed the connection between the baroclinic flow and the Lorenz-84 model. Niklas¹⁰ demonstrated the existence of bifurcations and strange attractors in a climate-related system. Persson¹¹ discussed Hadley's principle in understanding the trade winds. Lucarini, et al. 12 demonstrated the parametric smoothness and self-scaling of the statistical properties of a minimal climate model. Frierson, et al.¹³ researched the width of the Hadley cell in a simple and comprehensive general circulation model. Freire, et al.¹⁴ discussed the multistability and intransitivity in the Lorenz-84 low-order atmospheric circulation model. Wang, et al. 15 provided a dynamical analysis of the Lorenz-84 atmospheric circulation model.

Model Equations

In this model, x represents the strength of the globally averaged westerly current, while y and z represent the strength of the cosine and sine phases of a chain of superposed waves. The model equations are

$$\frac{dx}{dt} = -y^2 - z^2 - ax + afc$$

$$\frac{dy}{dt} = xy - bxz - y + gc$$

$$\frac{dz}{dt} = bxy + xz - z$$

fc and gc are the bifurcation and control variables, while a and b have values of 0.25 and 4.

Bifurcation analysis

The MATLAB software MATCONT is used to perform the bifurcation calculations. Bifurcation analysis deals with multiple steady-states and limit cycles. Multiple steady states occur because of the existence of branch and limit points. Hopf bifurcation points cause limit cycles. A commonly used MATLAB program that locates limit points, branch points and Hopf bifurcation points is MATCONT^{16,17}. This program detects Limit points (LP), branch points (BP) and Hopf bifurcation points(H) for an ODE system

$$\frac{dx}{dt} = f(x, \alpha)$$

 $x \in \mathbb{R}^n$ Let the bifurcation parameter be α . Since the gradient is orthogonal to the tangent vector,

The tangent plane at any point $W = [W_1, W_2, W_3, W_4, ..., W_{n+1}]$ nust satisfy

$$Aw = 0$$

Where A is

$$A = [\partial f / \partial x | |\partial f / \partial \alpha]$$

where $\partial f / \partial x$ is the Jacobian matrix. For both limit and branch points, the Jacobian matrix $J = [\partial f / \partial x]$ must be singular.

For a limit point, there is only one tangent at the point of singularity. At this singular point, there is a single non-zero vector, y, where Jy=0. This vector is of dimension n. Since there

is only one tangent the vector $y = (y_1, y_2, y_3, y_4, ... y_n)$ must align with $\hat{w} = (w_1, w_2, w_3, w_4, ... w_n)$. Since

$$J\hat{w} = Aw = 0$$

the n+1 th component of the tangent vector $W_{n+1} = 0$ at a limit point (LP).

For a branch point, there must exist two tangents at the singularity. Let the two tangents be z and w. This implies that

$$Az = 0$$
$$Aw = 0$$

Consider a vector v that is orthogonal to one of the tangents (say w). v can be expressed as a linear combination of z and w ($v = \alpha z + \beta w$). Since Az = Aw = 0; Av = 0 and since

w and v are orthogonal, $w^Tv=0$. Hence $Bv=\begin{bmatrix}A\\w^T\end{bmatrix}v=0$ which implies that B is singular.

Hence, for a branch point (BP) the matrix $B = \begin{bmatrix} A \\ w^T \end{bmatrix}$ must be singular.

At a Hopf bifurcation point,

$$\det(2f_x(x,\alpha)@I_n)=0$$

@ indicates the bialternate product while I_n is the n-square identity matrix. Hopf bifurcations cause limit cycles and should be eliminated because limit cycles make optimization and control tasks very difficult. More details can be found in Kuznetsov¹⁸⁻²⁰.

Hopf bifurcations cause limit cycles. The tanh activation function (where a control value u is replaced by) ($u \tanh u / \varepsilon$) is used to eliminate spikes in the optimal control profiles²¹⁻²⁴. Sridhar²⁵ explained with several examples how the activation factor involving the tanh function also eliminates the Hopf bifurcation points. This was because the tanh function increases the oscillation time period in the limit cycle.

Multiobjective Nonlinear Model Predictive Control (MNLMPC)

The rigorous multiobjective nonlinear model predictive control (MNLMPC) method developed by Flores Tlacuahuaz, et al.²⁶ was used.

Consider a problem where the variables $\sum_{i=t_f}^{t_i=t_f} q_i(t_i)$ (j=1, 2...n) have to be optimized simultaneously for a dynamic problem

$$\frac{dx}{dt} = F(x, u)$$

 t_f being the final time value and n the total number of objective variables and u the control parameter. The single objective optimal control problem is solved individually

optimizing each of the variables $\sum_{t_{i=0}}^{t_i=t_f} q_j(t_i)$ The optimization

of
$$\sum_{t_{i=0}}^{t_i=t_f} q_j(t_i)$$
 will lead to the values q_j^* . Then, the

multiobjective optimal control (MOOC) problem that will be solved is

$$\min\left(\sum_{j=1}^{n} \left(\sum_{t_{i=0}}^{t_i=t_f} q_j(t_i) - q_j^*\right)\right)^2$$
subject to $\frac{dx}{dt} = F(x, u)$;

This will provide the values of u at various times. The first obtained control value of u is implemented and the rest are discarded. This procedure is repeated until the implemented and the first obtained control values are the same or if the Utopia

point where (
$$\sum_{t_{i=0}}^{t_i=t_f} q_j(t_i) = q_j^*$$
 for all j) is obtained.

Pyomo²⁷ is used for these calculations. Here, the differential equations are converted to a Nonlinear Program (NLP) using the orthogonal collocation method
The NLP is solved using IPOPT²⁸ and confirmed as a global solution with BARON²⁹.

The steps of the algorithm are as follows

Optimize
$$\sum_{i=t_f}^{t_i=t_f} q_j(t_i)$$
 and obtain q_j^* .

Minimize
$$\left(\sum_{j=1}^{n} \left(\sum_{t_{i=0}}^{t_i=t_f} q_j(t_i) - q_j^*\right)\right)^2$$
 and get the control values

at various times.

Implement the first obtained control values.

Repeat steps 1 to 3 until there is an insignificant difference between the implemented and the first obtained value of the control variables or if the Utopia point is achieved. The Utopia

point is when
$$\sum_{t_{i=0}}^{t_i=t_f} q_j(t_i) = q_j^*$$
 for all j.

Sridhar³⁰ demonstrated that when the bifurcation analysis revealed the presence of limit and branch points the MNLMPC calculations to converge to the Utopia solution. For this, the singularity condition, caused by the presence of the limit or branch points was imposed on the co-state equation³¹. If the

minimization of q_1 lead to the value q_1^* and the minimization of q_2 lead to the value q_2^* . The MNLPMC calculations will minimize the function $(q_1-q_1^*)^2+(q_2-q_2^*)^2$. The multiobjective optimal control problem is

min
$$(q_1 - q_1^*)^2 + (q_2 - q_2^*)^2$$
 subject to $\frac{dx}{dt} = F(x, u)$

Differentiating the objective function results in

$$\frac{d}{dx_i}((q_1-q_1^*)^2+(q_2-q_2^*)^2)=2(q_1-q_1^*)\frac{d}{dx_i}(q_1-q_1^*)+2(q_2-q_2^*)\frac{d}{dx_i}(q_2-q_2^*)$$

The Utopia point requires that both $\left(q_{\rm l}-q_{\rm l}^*\right)$ and $\left(q_{\rm 2}-q_{\rm 2}^*\right)$ are zero. Hence

$$\frac{d}{dx_i}((q_1 - q_1^*)^2 + (q_2 - q_2^*)^2) = 0$$

The optimal control co-state equation is

$$\frac{d}{dt}(\lambda_i) = -\frac{d}{dx_i}((q_1 - q_1^*)^2 + (q_2 - q_2^*)^2) - f_x \lambda_i; \quad \lambda_i(t_f) = 0$$

 λ_i is the Lagrangian multiplier. t_f is the final time. The first term in this equation is 0 and hence

$$\frac{d}{dt}(\lambda_i) = -f_x \lambda_i; \lambda_i(t_f) = 0$$

At a limit or a branch point, for the set of ODE $\frac{dx}{dt} = f(x,u)$ f_x is singular. Hence there are two different vectors-values for $\left[\lambda_i\right]$ where $\frac{d}{dt}(\lambda_i) > 0$ and $\frac{d}{dt}(\lambda_i) < 0$. In between there is a vector $\left[\lambda_i\right]$ where $\frac{d}{dt}(\lambda_i) = 0$. This coupled with the boundary condition $\lambda_i(t_x) = 0$ will lead to $\left[\lambda_i\right] = 0$. This

boundary condition $\lambda_i(t_f) = 0$ will lead to $[\lambda_i] = 0$ This makes the problem an unconstrained optimization problem and the optimal solution is the Utopia solution.

Results and Discussion

When gc is the bifurcation parameter, a limit point and a Hopf bifurcation point were found at (x,y,z,gc) values of (0.655829, 0.038196, 0.291134, 0.776882)and (1.000144, 0, 0.011785, 0.047146). (**Figure 1a**). The limit cycle caused by this Hopf bifurcation point is shown in (**Figures 1b and 1c**). When gc was modified to gctanh(gc)/2.5, the Hopf bifurcation point disappears, but a limit point occurs at (x,y,z,gc) values of (0.089735, 0.443953, 0.175062, 1.339446).

The other parameters were a=1/4; b=4; fc=1.0007.

When fc is the bifurcation parameter, a limit point and a Hopf bifurcation point were found at (x,y,z,gc) values of label (0.786788, 0.021428, 0.316296, 1.188797) and (1.053891, -0.003032, 0.237177, 1.278940) (Figure 2a). The limit cycle caused by this Hopf bifurcation point is shown in (Figure 2b). When fc was modified to fctanh(gc)/0.1, the Hopf bifurcation point disappears (Figure 2c).

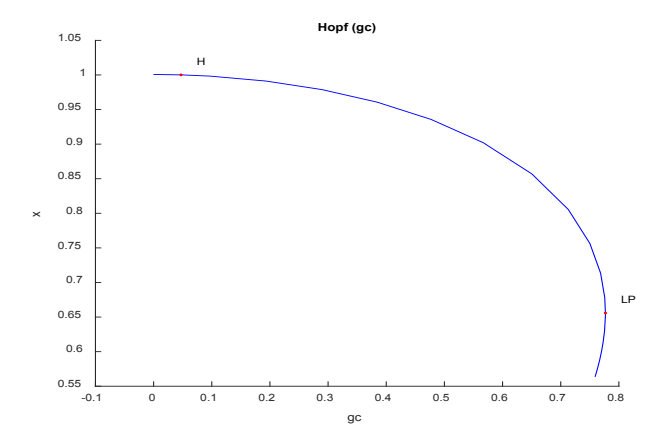


Figure 1a: Bifurcation diagram when gc is the bifurcation parameter (Hopf point occurs)

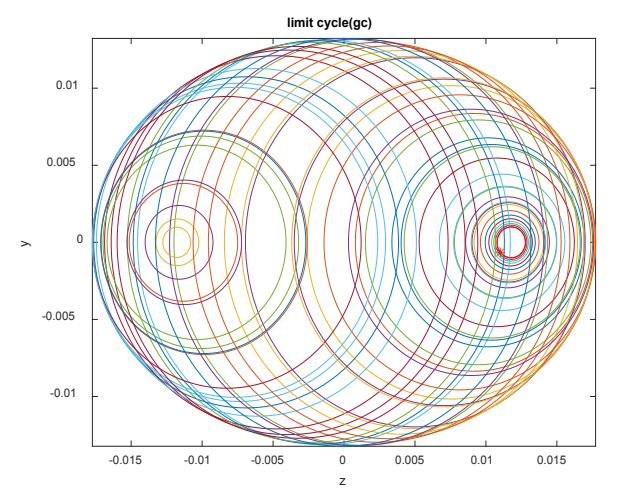


Figure 1b: Limit cycle when gc is the bifurcation parameter

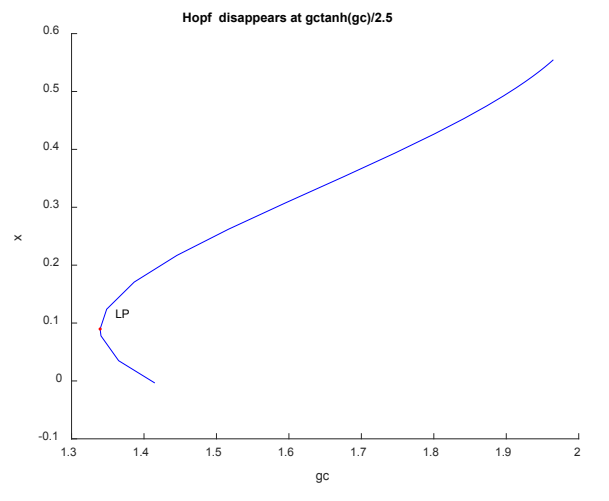


Figure 1c: Bifurcation diagram when gc is modified to gctanh(gc)/2.5 (Hopf point disappears).

The other parameters were a=1/4; b=4; gc=1.

In both cases, the use of the tanh activation factor eliminated the limit cycle causing Hopf bifurcation, validating the analysis in Sridhar²⁵.

For the MNLMPC calculations in model 1, $\sum_{t_{i=0}}^{t_i=t_f} x(t_i), \sum_{t_{i=0}}^{t_i=t_f} y(t_i), \sum_{t_{i=0}}^{t_i=t_f} z(t_i) \quad \text{were minimized individually}$ and each of them led to a value of 0. The overall optimal control problem will involve the minimization of

$$(\sum_{t_{i=0}}^{t_i=t_f} x(t_i))^2 + (\sum_{t_{i=0}}^{t_i=t_f} y(t_i))^2 + (\sum_{t_{i=0}}^{t_i=t_f} z(t_i))^2$$

was minimized subject to the equations governing the model. This led to a value of zero the Utopia.

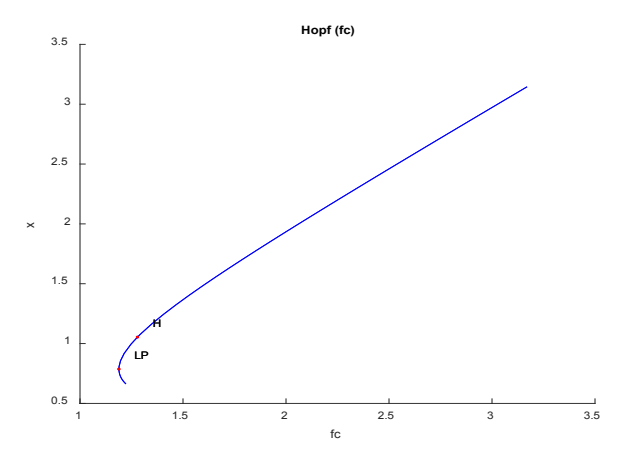


Figure 2a: Bifurcation diagram when fc is the bifurcation parameter (Hopf point occurs).

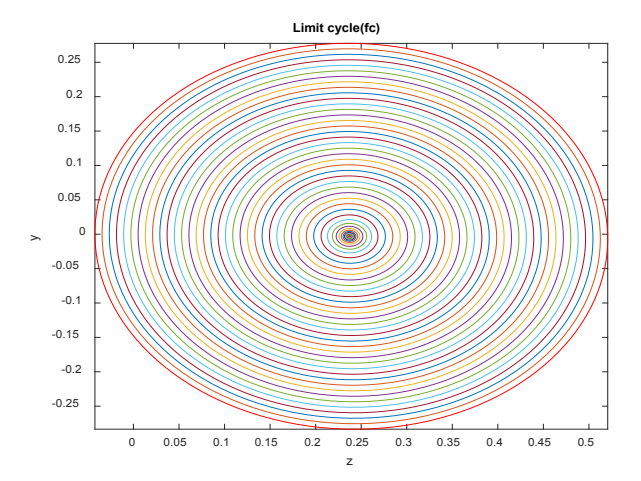


Figure 2b: Limit cycle when fc is the bifurcation parameter.

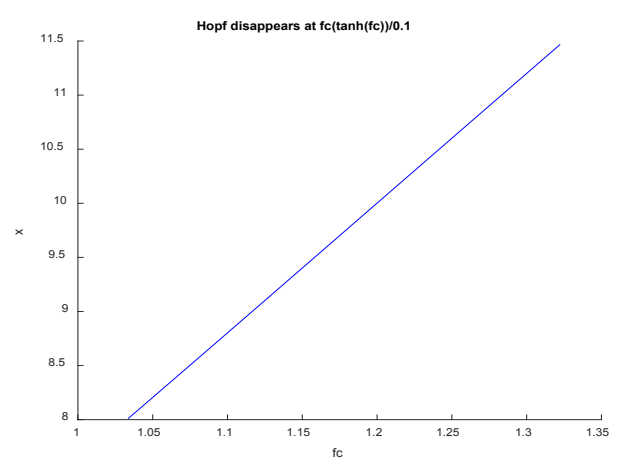


Figure 2c: When fc was modified to fctanh(gc)/0.1, the Hopf bifurcation point disappears.

The MNLMPC values of the control variables, fc and gc, were 0.8132 and 0.363. The various MNMPC figures are shown in **(Figures 3a-3d)**. The profiles of x y z fc and gc exhibited noise and this was remedied using the Savitzky-Golay filter. The

modified profiles of x, y, z, fc and gc were xsg, ysg, zsg.. fcsg and gcsg.

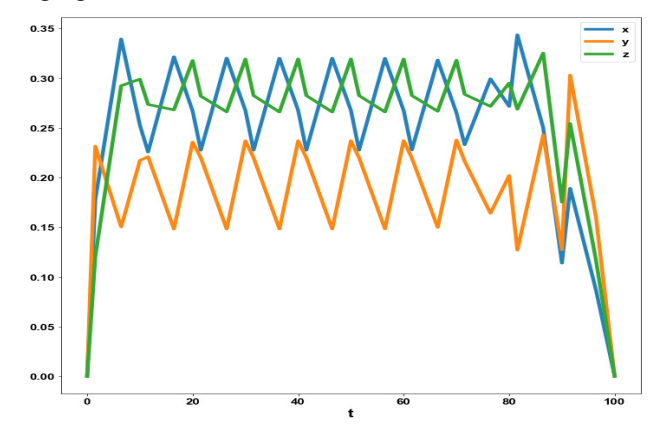


Figure 3a: MNLMPC; x, y, z profiles.

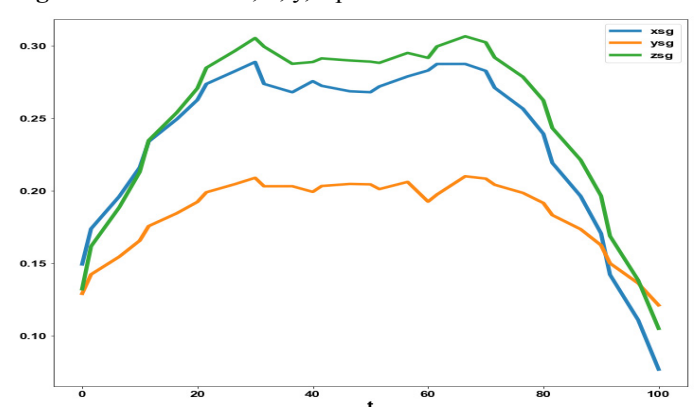


Figure 3b: MNLMPC; xsg, ysg, zsg profiles.

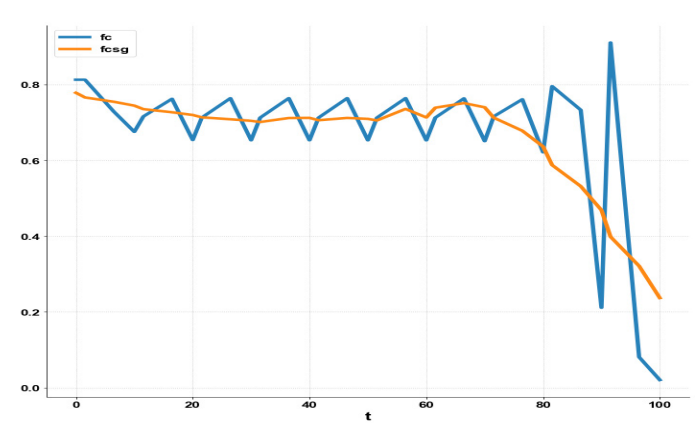


Figure 3c: MNLMPC; fc, fcsg profiles.

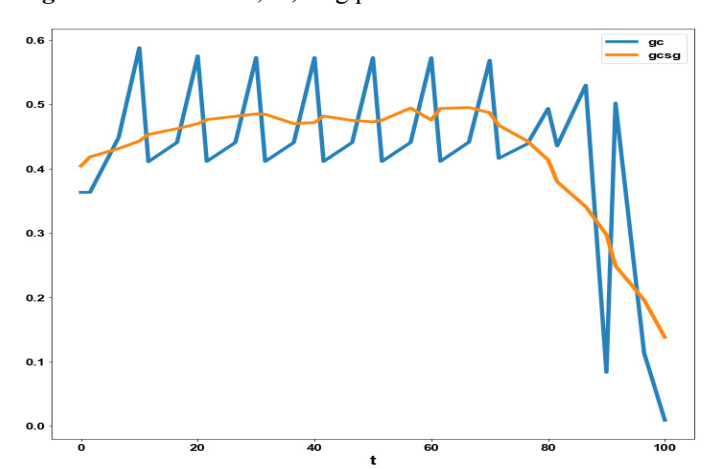


Figure 3d: MNLMPC; gc, gcsg profiles.

The presence of the limit and branch points is beneficial because it allows the MNLMPC calculations to attain the Utopia solution, validating the analysis of Sridhar³⁰.

Conclusions

Bifurcation analysis and multiobjective nonlinear control (MNLMPC) studies on the Lorenz-84 atmospheric circulation model. The bifurcation analysis revealed the existence of Hopf bifurcation points and limit points. The Hopf bifurcation point, which causes an unwanted limit cycle, is eliminated using an activation factor involving the tanh function. The limit points (which cause multiple steady-state solutions from a singular point) are very beneficial because they enable the Multiobjective nonlinear model predictive control calculations to converge to the Utopia point (the best possible solution) in the models. A combination of bifurcation analysis and Multiobjective Nonlinear Model Predictive Control (MNLMPC) for the Lorenz-84 atmospheric circulation model is the main contribution of this paper.

Data availability statement

All data used is presented in the paper.

Conflict of interest

The author, Dr. Lakshmi N Sridhar, has no conflict of interest.

Acknowledgement

Dr. Sridhar thanks Dr. Carlos Ramirez and Dr. Suleiman for encouraging him to write single-author papers

References

- Nicolis C. Solar variability and stochastic effects on climate. Solar Physics 1981;74(2):473-478.
- 2. Benzi R, Parisi G, Sutera A, Vulpiani A. Stochastic resonance in climate change. Tellus 1982;34:10-16.
- 3. Nicolis C. Stochastic aspects of climatic transitions-response to a periodic forcing. Tellus 1982;34:1-9.
- 4. Lorenz EN. Irregularity: a fundamental property of the atmosphere. Tellus A 1984;36(2):98-110.
- Shilnikov A, Nicolis G, Nicolis C. Bifurcation and predictability analysis of a low-order atmospheric circulation model. Int J Bifurcation and Chaos in App Sci Eng 1995;5(6):1701-1711.
- Roebber PJ. Climate variability in a low-order coupled atmosphere-ocean model. Tellus A 1995;47(4):473-494.
- Pelino V, Pasini A. Dissipation in Lie-Poisson systems and the Lorenz-84 model. Physics Letters A: General, Atomic and Solid-State Physics 2001;291(6):389-396.
- Broer H, Sim'o C, Vitolo R. Bifurcations and strange attractors in the Lorenz-84 climate model with seasonal forcing. Nonlinearity 2002;15(4):1205-1267.
- Van Veen L. Baroclinic flow and the Lorenz-84 model. Int J Bifurcation and Chaos in App Sci Eng 2003;13(8):2117-2139.
- Niklas L. Bifurcations and strange attractors in a climate-related system. Differential Equations and Control Processes 2005;1:1-53.
- Persson A. Hadley's principle: understanding and misunderstanding the trade winds. History of Meteorology 2006;3:17-42.
- 12. Lucarini V, Speranza A, Vitolo R. Parametric smoothness and self-scaling of the statistical properties of a minimal climate

- model: what beyond the mean field theories? Physica D: Nonlinear Phenomena 2007;234(2):105-123.
- Frierson DMW, Lu J, Chen G. Width of the Hadley cell in simple and comprehensive general circulation models. Geophysical Research Letters 2007;34(18).
- Freire JG, Bonatto C, DaCamara CC, Gallas JA. Multistability, phase diagrams and intransitivity in the Lorenz-84 low-order atmospheric circulation model. Chaos 2008;18(3):8.
- Hu W, Uang Y, Guoguang W. Dynamical Analysis of the Lorenz-84 Atmospheric Circulation Model. J App Mathematics 2014:1-15.
- Dhooge A, Govearts W, Kuznetsov AY. MATCONT: A Matlab package for numerical bifurcation analysis of ODEs. ACM transactions on Mathematical software 2003;29(2):141-164.
- Dhooge A, Govaerts W, Kuznetsov YA, Mestrom W, Riet AM. CL MATCONT; A continuation toolbox in Matlab 2004.
- Kuznetsov YA. Elements of applied bifurcation theory. Springer, NY 1998.
- Kuznetsov YA. Five lectures on numerical bifurcation analysis. Utrecht University, NL 2009.
- Govaerts WJF. Numerical Methods for Bifurcations of Dynamical Equilibria. SIAM 2000.
- Dubey SR, Singh SK, Chaudhuri BB. 2022 Activation functions in deep learning: A comprehensive survey and benchmark. Neurocomputing 2022;503:92-108.
- Kamalov AF, Safaraliev NM, Cherukuri AK, Zgheib R. Comparative analysis of activation functions in neural networks. 28th IEEE Int Conf on Electronics, Circuits and Systems (ICECS) 2021:1-6.

- Szandała T. Review and Comparison of Commonly Used Activation Functions for Deep Neural Networks. ArXiv 2020.
- Sridhar LN. Bifurcation Analysis and Optimal Control of the Tumor Macrophage Interactions. Biomed J Sci Tech Res 2023;53(5).
- Sridhar LN. Elimination of oscillation causing Hopf bifurcations in engineering problems. J App Math 2024;2(4):1826.
- Flores-Tlacuahuac, A. Pilar Morales, Toledo MR. Multiobjective Nonlinear model predictive control of a class of chemical reactors. I & EC research 2012:5891-5899.
- 27. William HE, Laird CD, Watson JP, et al. Siirola. Pyomo Optimization Modeling in Python Second Edition 67.
- Wächter A, Biegler L. On the implementation of an interiorpoint filter line-search algorithm for large-scale nonlinear programming. Math Program 2006;106:25-57.
- 29. Tawarmalani M, Sahinidis NV. A polyhedral branch-and-cut approach to global optimization. Mathematical Programming 2005;103(2):225-249.
- Sridhar LN. Coupling Bifurcation Analysis and Multiobjective Nonlinear Model Predictive Control. Austin Chem Eng 2024;10(3):1107.
- 31. Upreti, Simant Ranjan. Optimal control for chemical engineers. Taylor and Francis 2013.